2014 International Conference on Unmanned Aircraft Systems (ICUAS)
May 27-30, 2014. Orlando, FL, USA

Decision Strategies for Automated Visual Collision Avoidance

Aaron Mcfadyen*, Adrien Durand-Petiteville** and Luis Mejias*

Abstract— **This paper provides a preliminary analysis of an autonomous uncooperative collision avoidance strategy for unmanned aircraft using image-based visual control. Assuming target detection, the approach consists of three parts. First, a novel decision strategy is used to determine appropriate reference image features to track for safe avoidance. This is achieved by considering the current rules of the air (regulations), the properties of spiral motion and the expected visual tracking errors. Second, a spherical visual predictive control (VPC) scheme is used to guide the aircraft along a safe spiral-like trajectory about the object. Lastly, a stopping decision based on thresholding a cost function is used to determine when to stop the avoidance behaviour. The approach does not require estimation of range or time to collision, and instead relies on tuning two mutually exclusive decision thresholds to ensure satisfactory performance.**

I. Introduction

Autonomous technologies for Unmanned Aircraft Systems (UAS) such as Failsafe and Fault-Tolerant Systems, See and Avoid and Emergency Landing are being recognised as critical capabilities for the integration and routine operation of UAS into the national airspace [1], [2], [3]. Operations in civilian airspace imply sharing the sky with other aircraft, and often require flight over restricted or populated areas. A major accident could therefore have significant repercussions regarding public acceptance of unmanned aircraft systems. One way to minimise such risks, is to increase the level of automation onboard UAS platforms. As such, this paper is devoted to automated See and Avoid technology by introducing novel decision and control strategies. The approach is suitable for uncooperative encounters and does not rely on estimating range or time to collision.

See and Avoid capability refers to the short term, reactive collision avoidance conducted by pilots in response to immediate threats. It involves the pilots visual system, recollection of regulatory procedures and pilot knowledge and skill. Considering that a pilot's ability to adequately See and Avoid has also been deemed questionable [4], [5], [6], attempting to replicate pilot behaviour presents a number of difficult technical and operational challenges. Research has therefore focused on how an automated system may be able to aid, augment or replace the pilot completely.

Strictly speaking, the uncooperative nature of See and Avoid and the reliance on pilot vision implies electro-optic sensors should be used for obstacle detection. Fortunately, this means that despite typical size, weight and power constraints on some UAS, a collision avoidance system leveraging computer vision may be used on multiple platforms. Unfortunately, this restricts the state information that can be obtained reliably, such as object range or time to collision. This is due to the fact that a conflicting aircraft appears as a small, slow moving, low contrast object that does not significantly change shape or size until seconds before impact [7], [8], [9], [10], [11]. Considering the limited avoidance time available, unknown object size and relative geometry (scale), techniques based on optic flow, passive ranging and stereo vision will likely fail [12], [13], [14], [15], [16], [17]. Such constraints have prompted the development of new techniques for object detection, tracking, estimation and control. To this end, the following contributions are proposed in this paper:

1) Introduction of a novel vision-based avoidance decision strategy for both static and constant velocity targets using the properties of conical spirals, rules of the air and the expected uncertainty on image feature measurements.
2) Improvements to a flight-tested spherical visual predictive control scheme for collision avoidance that better approximates spiral motion, and provides an indication of when to stop avoidance behaviour.

This paper is structured as follows. Section II provides the problem background including relevant literature. Conical spiral dynamics for both static and dynamic objects are outlined in section III, providing the bases for the collision avoidance approach. In Section IV, the avoidance decision strategy, spherical visual predictive controller and resolution (stopping) strategy is presented. As a precursor to implementation on larger unmanned aircraft, Section V provides some preliminary simulation results for multiple conflict and non-conflict encounters using a small rotorcraft platform.

II. Background

Vision-based control describes control systems in which feedback is derived by processing measurements from image-features [18]. Position-based visual servoing (PVBS) uses such measurements to estimate relative state and subsequently control the vehicle in the task space. Image based-visual servoing (IBVS) uses the image feature measurements (or estimates) directly for feedback, such that control is performed with respect to the image space. Image-based approaches are well suited to collision avoidance, given its reactive nature and inherent robustness to range uncertainty.

However, many existing image-based collision avoidance systems do not realistically consider the See and Avoid

*Australian Research Centre for Aerospace Automation (ARCAA), School of Electrical Engineering and Computer Science, Queensland University of Technology (QUT), Brisbane, Australia. aaron.mcfadyen@qut.edu.au

**CyPhy Laboratory, School of Electrical Engineering and Computer Science, Queensland University of Technology (QUT), Brisbane, Australia

978-1-4799-2376-2/14/$31.00 ©2014 IEEE

operational environment and associated constraints. Camera field of view issues may not be addressed and range or time to collision estimates may be required. They may be used either in the controller, or to determine when to start and stop avoidance. What is required, is a system that determines where to move the image features to ensure collision avoidance, before deciding when to stop the visual control and resume regular flight. A large field of view would also be needed to help replicate the pilots visual system.

If a vehicle moves at constant forward speed whilst holding an object at a fixed angular position (in the sensor field of view), the resulting motion approximates a conical spiral trajectory about the object. Previously, such spirals[1] have been used to model the flight of insects and raptors [19], [20]. Recently, the concept has been used either implicitly [21], [22], [23] or explicitly [24], [25], [26] for vision-based collision avoidance in which limited state information is available. As such, attempts have been made to simultaneously acquire better state information whilst ensuring collision avoidance [27], [28], [29]. Importantly, the control that optimizes range observability forces the establishment of a circular spiral. To account for problem constraints, nonlinear model predictive control theory [30] has recently been used to derive visual predictive control [31] approaches [32]. Visibility, state and control constraints can be explicitly considered in the control design whilst guiding a safe spiral-like avoidance path [33], [34]. In most cases, static objects are considered while dynamic objects are managed under simplifying assumptions or for a subset of collision geometries. The reference spiral is either fixed or chosen according to the image position of the object upon initial detection. In this respect, the avoidance decision for image-based approaches remains relatively immature.

In an automated system, and independent of the collision avoidance method, it should be noted that avoidance does not directly imply the conflict has been resolved. Often this is assumed, but realistically a decision criteria would be required to stop the avoidance behaviour. This is often neglected as it is considered less critical to safety. However, if a system does not successfully resolve conflicts, it may be considered inadequate as operator intervention may be consistently required.

III. Conical Spirals

To perform collision avoidance, this paper proposes that the aircraft has to attempt to visually establish and track a spiral defined with respect to the obstacle. In this section, we first present the spiral equations with respect to a static obstacle followed by those for a dynamic obstacle. We then provide a direct relationship between the conical spiral angles and the spherical image features used to represent the objects image position.

[1]Also referred to as equiangular spirals, conchospirals or logarithmic spirals

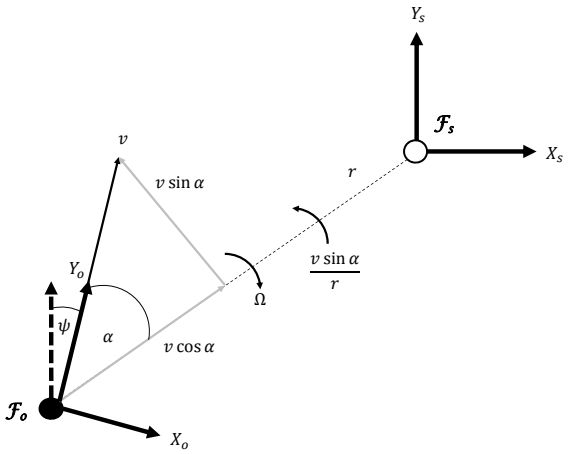

Fig. 1. Spiral geometry for static obstacle (apex)

A. Static Apex

Consider a frame $\mathcal{F}_O$ moving with a constant speed v with respect to a reference frame $\mathcal{F}_S$, where the object (apex) coincides with the origin of $\mathcal{F}_S$. The reference frame $\mathcal{F}_S$ can be viewed like a fixed world frame, whose origin is shifted according to the object position. The orientation of $\mathcal{F}_O$ is controlled using a yaw angular velocity Ω. The bearing angle α is defined as the angle between the projection of the velocity vector onto the xy-plane in $\mathcal{F}_S$ and the apex such that $\alpha \in [-\pi,\ \pi]$. The elevation angle β is defined as the angle between the xy-plane of $\mathcal{F}_S$ and the velocity vector such that $\beta \in [-\pi/2,\ \pi/2]$. The range r denotes the distance between the origins of the two frames. The heading of the vehicle ψ is measured with respect to the world frame and its speed is defined as the magnitude of the velocity vector such that $v = (v_x^2 + v_y^2 + v_z^2)^{\frac{1}{2}}$. An example of the geometry is shown in Fig 1 where $\mathcal{F}_O$ moves in the $xy-$plane of $\mathcal{F}_S$ such that $\beta = 0$. The nonlinear system of ordinary differential equations describing the vehicle motion then becomes

$$\dot{r}(t) = -v\cos\alpha(t) \quad (1)$$

$$\dot{\alpha}(t) = \frac{v\sin\alpha(t)}{r(t)} - \Omega(t) \quad (2)$$

$$\dot{\psi}(t) = \Omega(t) \quad (3)$$

Provided the sampling time T_s is sufficiently small, the system can be approximated in discrete time as

$$r_{k+1} = r_k - T_s v\cos\alpha_k \quad (4)$$

$$\alpha_{k+1} = \alpha_k + T_s\left(\frac{v\sin\alpha_k}{r_k} - \Omega_k\right) \quad (5)$$

$$\psi_{k+1} = \psi_k + T_s\Omega_k \quad (6)$$

Consider the case where the relative bearing angle α is constant $\forall\, k$. Based on equation (4), it can be deduced that for $||\alpha|| = \pi/2$ the range is constant, whereas for $||\alpha|| > \pi/2$ the range increases. For $||\alpha|| < \pi/2$ the range decreases, with $\alpha = 0$ denoting a degenerate case whereby motion is directly toward the object. Lateral separation can therefore be assured for all $||\alpha|| \geq \pi/2$. Some example trajectories are illustrated in Fig. 2.

Now consider the case where $\beta \neq 0$. The resulting trajectory will be a 3 dimensional spiral that circumvents the surface of a cone whose opening angle is defined by β. As such, vertical separation from the object can be assured for all non-zero β, provided $||\alpha|| \geq \pi/2$.

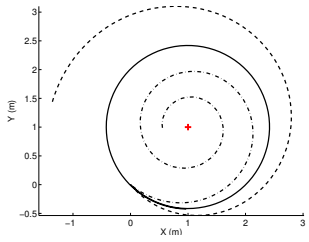

Fig. 2. Example trajectories of $\mathcal{F}_O$ in $\mathcal{F}_S$ for a static reference point (*red*) with $\alpha = \pi/2$ (-), $\alpha = 33\pi/32$ (- -) and $\alpha = 31\pi/32$ (- ·). Initial aircraft and obstacle positions are $(0, 0)$ and $(1, 1)$ respectively.

B. Dynamic Apex

For dynamic objects, the reference frame $\mathcal{F}_S$ is now moving with a constant velocity v_t and fixed heading Φ. Again, consider the case where motion of $\mathcal{F}_O$ is in the $xy-$plane of $\mathcal{F}_S$ such that $\beta = 0$. An example of the geometry is shown in Fig 3. The nonlinear system of ordinary differential equations describing the motion is given by

$$\dot{r}(t) = -v\cos\alpha(t) + v_t\cos(\psi(t) + \alpha(t) - \Phi) \quad (7)$$

$$\dot{\alpha}(t) = \frac{v\sin\alpha(t) - v_t\sin(\psi(t) + \alpha(t) - \Phi)}{r(t)} - \Omega(t) \quad (8)$$

$$\dot{\psi}(t) = \Omega(t) \quad (9)$$

which in discrete time can be approximated as

$$r_{k+1} = r_k + T_s(v_t\cos(\psi_k + \alpha_k - \Phi) - v\cos\alpha_k) \quad (10)$$

$$\alpha_{k+1} = \alpha_k + T_s\left(\frac{v\sin\alpha_k - v_t\sin(\psi_k + \alpha_k - \Phi)}{r_k} - \Omega_k\right) \quad (11)$$

$$\psi_{k+1} = \psi_k + T_s\Omega_k \quad (12)$$

Based on the previous analysis, consider the case where $\alpha = \pi/2 \quad \forall\, k$, and $||v|| > ||v_t||$. Some example trajectories are illustrated in Fig. 4. Although there is no guarantee that the range will not decrease as in the static case, the two frames will not collide. Now consider the case where $||v|| \leq ||v_t||$ and an attempt is made to track a spiral where $\alpha = \pi/2 \quad \forall\, k$. Some example trajectories are illustrated in Fig. 5 for $\Phi \in (\pi,\ 2\pi)$. In this case, it is impossible to maintain a spiral, shown by the divergent paths about the object position and inability to encompass the object within a complete rotation. However, in attempting to maintain the reference spiral, α increases as the vehicle moves toward a safer location. Issues could arise for $\Phi \in (0,\ \pi)$ whereby the bearing angle initially decreases such that $-\pi/2 < \alpha < \pi/2$, resulting in an unsafe trajectory. A similar situation occurs for $\Phi \in (\pi,\ 2\pi)$ and a reference spiral defined by $\alpha \leq -\pi/2$. Considering the inclusion of the relative elevation angle β, any non-zero value means the object is not at the same level as the vehicle. Similar to the static case, vertical separation can thus be assured.

The analysis indicates that both lateral and vertical collision avoidance of constant velocity obstacles is possible by

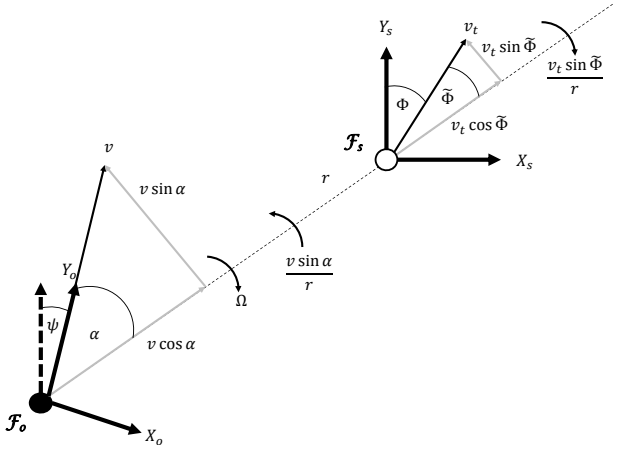

Fig. 3. Spiral geometry for dynamic obstacle (apex) where $\tilde{\Phi} = \psi + \alpha - \Phi$

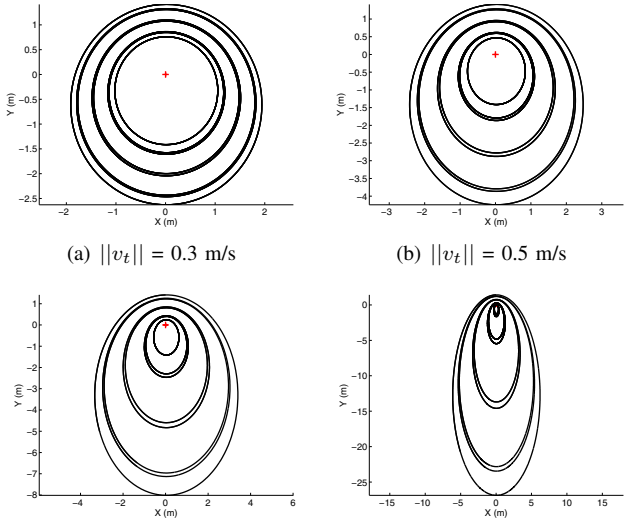

(a) $||v_t||$ = 0.3 m/s (b) $||v_t||$ = 0.5 m/s

(c) $||v_t||$ = 0.7 m/s (d) $||v_t||$ = 0.9 m/s

Fig. 4. Example trajectories of $\mathcal{F}_O$ in $\mathcal{F}_S$ for $\alpha = \pi/2$ and $||v||$ = 1 m/s. From the center to exterior the objects heading Φ in $\mathcal{F}_S$ is $0, \pi/4, \pi/2, 3\pi/4, \pi, 5\pi/4, 3\pi/2, 7\pi/4$. Initial aircraft and obstacle position are $(1, 1)$ and $(0, 0)$ respectively.

attempting to establish and track a spiral such that $||\alpha|| \geq \pi/2$ and $\beta \neq 0$. The difficulty relies in determining the orientation of the reference spiral to track ($\alpha \pm \pi/2$), given the unknown intent of the object. An avoidance decision is thus required upon initial detection to help determine the exact reference spiral to track.

C. Relevance

The preceding analysis suggests that collision avoidance of both static and constant velocity obstacles is possible by tracking appropriate elevation and bearing angles to the object. Specifically, $||\alpha|| \geq \pi/2$ and $\beta \neq 0$. However, to track a spiral using image-based control a relationship must be derived between these conical angles and the observed image features. Considering the requirements for a large field of view and the representation of the conical angles, a spherical camera model is a natural choice [35], [36].

Using the spherical model, an image point can be represented by a colatitude σ and azimuth γ angle such that

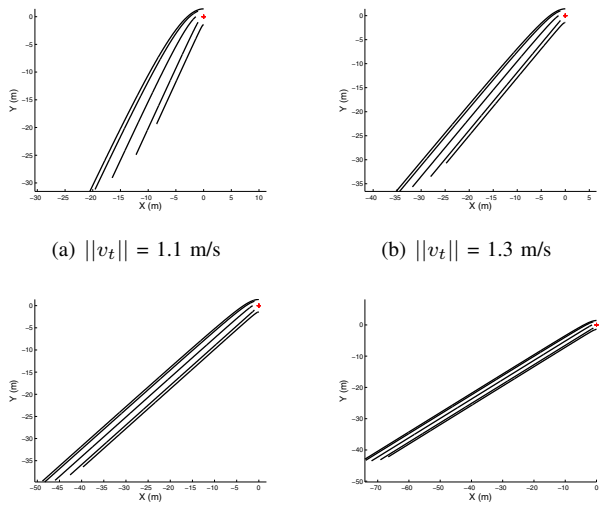

(a) $||v_t||$ = 1.1 m/s (b) $||v_t||$ = 1.3 m/s

(c) $||v_t||$ = 1.5 m/s (d) $||v_t||$ = 1.9 m/s

Fig. 5. Example trajectories of $\mathcal{F}_O$ in $\mathcal{F}_S$ for $\alpha = \pi/2$ and $||v||$ = 1 m/s. From the center to exterior the objects heading Φ in the world frame is $0, 7\pi/4\pi, 3\pi/2, 5\pi/4\pi$. Initial aircraft and obstacle position in the world frame are $(0, 0)$ and $(1, 1)$ respectively

$\sigma \in [0,\ \pi]$ and $\gamma \in [-\pi,\ \pi]$. Consider a spherical camera frame $\mathcal{F}_C$ rigidly attached to the aircraft and observing a point object $\mathbf{p}$. The object, considered to be the conical apex, can be expressed in the camera frame as ${}^c\mathbf{p}$ such that

$$ {}^c\mathbf{p}(t) = \begin{pmatrix} X(t) \\ Y(t) \\ Z(t) \end{pmatrix} = \begin{pmatrix} r(t)S\sigma(t)C\gamma(t) \\ r(t)S\sigma(t)S\gamma(t) \\ r(t)C\sigma(t) \end{pmatrix} = r(t){}^c\tilde{\mathbf{p}}(t) \tag{13} $$

where $C = \cos(\cdot)$, $S = \sin(\cdot)$ and a tilde denotes a unit vector. Due to offsets in camera mounting position, the origins of $\mathcal{F}_C$ and $\mathcal{F}_O$ are displaced by the vector ${}^o\mathbf{t}_c$. The orientation of $\mathcal{F}_C$ with respect to $\mathcal{F}_O$ is such that ${}^oR_c$ defines a rotation from $\mathcal{F}_C$ to $\mathcal{F}_O$. Expressing the object position in $\mathcal{F}_O$, (13) becomes

$$ {}^o\mathbf{p}(t) = {}^oR_c{}^c\mathbf{p}(t) + {}^o\mathbf{t}_c \tag{14} $$

$$ r(t){}^o\tilde{\mathbf{p}}(t) = r(t){}^oR_c{}^c\tilde{\mathbf{p}}(t) + {}^o\mathbf{t}_c \tag{15} $$

Dividing through by $r(t)$ and assuming $r(t) \gg \|{}^o\mathbf{t}_c\|$

$$ {}^o\tilde{\mathbf{p}}(t) = {}^oR_c(t){}^c\tilde{\mathbf{p}}(t) \tag{16} $$

Substituting for $\mathbf{p}$ using spherical coordinates

$$ \begin{pmatrix} C\beta'(t)C\alpha(t) \\ C\beta'(t)S\alpha(t) \\ S\beta'(t) \end{pmatrix} = {}^oR_c \begin{pmatrix} S\sigma(t)C\gamma(t) \\ S\sigma(t)S\gamma(t) \\ C\sigma(t) \end{pmatrix} \tag{17} $$

where

$$ {}^oR_c(t) = R(\theta)\ R(\phi) \tag{18} $$

$$ {}^oR_c(t) = \begin{pmatrix} C\theta(t) & S\theta(t)S\phi(t) & C\phi(t)S\theta(t) \\ 0 & C\phi(t) & -S\phi(t) \\ -S\theta(t) & C\theta(t)S\phi(t) & C\theta(t)C\phi(t) \end{pmatrix} \tag{19} $$

$$ \beta' = \beta - \pi/2 \tag{20} $$

The camera pitch and roll angles are denoted by $\theta(t)$ and $\phi(t)$ respectively whilst β' denotes a shifted version of the elevation angle. The conical angles can then be estimated by solving (17) using the measured spherical image features and vehicle orientation. By using a spherical camera and applying this de-rotation, any spiral may be visually tracked regardless of the vehicle dynamics and viewing angle. Applying the de-rotation before any image-based control means the image features $\mathbf{s} = [\sigma\ \gamma]$ will correspond to the shifted conical angles $\mathbf{c} = [\beta'\ \alpha]$. As such, the reference image features would be the same as the reference conical angles $\mathbf{c}^* \approx \mathbf{s}^*$, and thus directly determine the reference spiral. If the image feature are not de-rotated before image-based control is applied, $\mathbf{s}^* \neq \mathbf{c}^*$.

IV. Decision, Control and Logic

Assuming object detection, the collision avoidance approach contains three parts; an avoidance decision, control action and a resolution decision. The avoidance decision strategy determines which spiral to follow. The controller is then used to track the reference spiral. The resolution decision or stopping criteria is required to cease avoidance behaviour. In this paper, a small quadrotor model and an experimentally validated controller is used, but the strategy can be extended to any aircraft provided a dynamic model can be determined. The approach is summarized in Fig. 6.

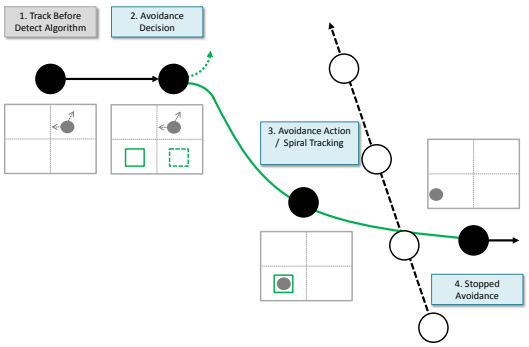

Fig. 6. Collision avoidance strategy. Assuming object detection (*grey*), a safe spiral is selected (*blue boxes*) and the conflict is avoided (*green line*)

A. Avoidance Decision - Establishing Spirals

It has been suggested that humans detect a collision by primarily considering the relative angular rate [37] with respect to the object. Applying this theory to aircraft collision avoidance however, bearing rate alone has proved insufficient to initially distinguish between collision and non collision targets [38]. This is likely due to uncertainty on image feature measurements and subsequent estimates of relative bearing [39]. In this case, and by considering the short duration of the encounters, it may be best to always act. The difficulty is in determining the direction of the action to take and therefore, which exact spiral to attempt to establish. Some indication is given by the analysis in the previous section, suggesting a spiral defined by $\gamma^* \pm \pi/2$ and $\sigma^* - \pi/2 \neq 0$ should be established. However, this should be considered in conjunction

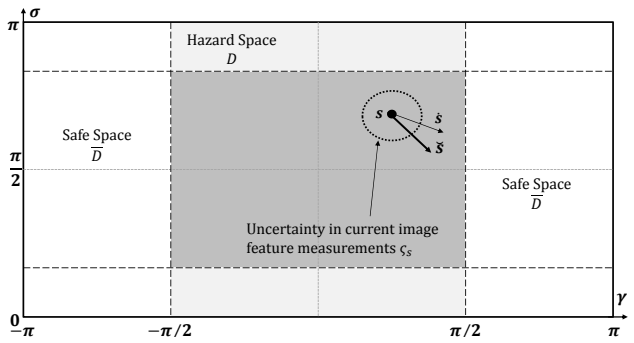

Fig. 7. Example planar representation of the spherical imaging surface, including an example object, bounded uncertainty on the image feature measurements ς_s and danger area D.

with the rules of the air [40]. Although these rules may not result in geometrically optimal behaviour or ensure collision, they need to be considered given the airspace is shared with manned aircraft. This ensures unmanned aircraft behaviour in a conflict is more predictable from a pilots perspective.

Consider the image feature position $\mathbf{s} = [\sigma \ \gamma]$, image feature rate $\dot{\mathbf{s}} = [\dot{\sigma} \ \dot{\gamma}]$ and a danger zone D defined by any image position in the region $-\pi/2 < \gamma < \pi/2$ as shown in Fig. 7. At the initial detection instant k_d, a decision criteria to move left or right and up or down is required. This is achieved by analysing the products $\breve{\sigma} = \sigma \cdot \dot{\sigma}$ and $\breve{\gamma} = \gamma \cdot \dot{\gamma}$, the expected uncertainty on the image feature measurements $\varsigma = [\varsigma_s \ \varsigma_{\dot{s}}]$, and the rules of the air (see Appendix). A qualitative measure of the rate of change of object size is assumed to determine if an object is being overtaken. Attributes such as image intensity about the object may be used to this end, but will require further investigation. Importantly, range or time to collision is not estimated, allowing the proposed avoidance decision strategy to be tuned using a single threshold $\eta = \varsigma_s \cdot \varsigma_{\dot{s}}$, representing the confidence in the image feature estimates.

Algorithm 1 Avoidance Decision Strategy - Colatitude

```
Set σ = σ − π/2,   σ*_o = 35π/180
if Object Above Horizontal then
    if σ̆ > η then                                  ▷ Divergent Features
        σ* = π/2 + σ*_o                            ▷ **No Crossing
    else if σ̆ < −η then                            ▷ Convergent Features
        σ* = π/2 − σ*_o                            ▷ **Allow Crossing
    else                                           ▷ Static or Centerline Features
        if Overtaking then                         ▷ Overtaking
            σ* = σ                                 ▷ **No Movement
                                                   CAR 162(4)
        elseNot Overtaking
            σ* = π/2 − σ*_o                        ▷ **Allow Crossing
        end if
    end if
else Below Above Horizontal
    Reciprocal Logic
end if
```

** Aircraft Action

Important to note that many reference colatitude angles could be chosen. A colatitude reference is selected by considering the nonlinearity of the reference position and the expectations on stability and feasibility [34]. In this way, there is better assurance the reference feature will be tracked from a control perspective. Recalling $\sigma \in [0, \pi]$, it is useful to define a safe reference offset value σ_o^* from the horizontal image centreline in order to determine σ^*. The avoidance decision strategies for colatitude σ and azimuth γ are given in algorithm 1 and 2 respectively.

Although the performance will vary depending on η, by using a single decision threshold the approach lends itself to probabilistic analysis techniques, which will be required for any subsequent system certification.

Algorithm 2 Avoidance Decision Strategy - Azimuth

```
if γ ∈ D then                                      ▷ Danger Area
    if γ̆ < η then                                  ▷ Convergent, Centreline or Static Features
        γ* = −π/2                                  ▷ **Allow Crossing
                                                   Right-of-Way Rules, CAR 162(1-4)
    else                                           ▷ Divergent Features
        if γ < 0 then                              ▷ Left Centreline
            γ* = −π/2                              ▷ **No Crossing
        else                                       ▷ Right Centreline
            γ* = π/2                               ▷ **No Crossing
        end if
    end if                                         ▷ Static or Centerline Features
else                                               ▷ Outside Danger Area
    γ* = γ                                         ▷ **No Movement
end if
```

** Aircraft Action

B. Control - Tracking Spirals

Visual Predictive Control (VPC) schemes are derived by casting the visual servoing problem into a nonlinear model predictive control (NMPC) framework. It allows explicit consideration of visibility, state and control constraints within the control design by combining a dynamic model of the vehicle and the image kinematics (image Jacobian). An optimal control is calculated and then applied at each time step by predicting the vehicle behaviour over a finite time horizon. A solution can be obtained sufficiently fast with modern solvers, allowing the consideration of complex dynamic systems such as vision-based aircraft controllers. The control scheme presented here is based on a partial quadrotor model using 2 degrees of freedom first derived in [33].

The vehicles states $\mathbf{z} = [\dot{z} \ \psi \ \omega]$ and image features $\mathbf{s} = [\sigma \ \gamma]$ are combined to form the system state vector $\mathbf{x} = [\mathbf{z} \ \mathbf{s}]$ where ω is the yaw rate, $\dot{z}$ is the vertical velocity and ψ is the yaw angle. The control vector $\mathbf{u} = [F \ \Omega]$ defines the system inputs where F is the thrust and Ω is a yaw rate command. The resulting dynamic model is defined in discrete time as $\mathbf{x}_{k+1} = \mathbf{f}(\mathbf{x}_k, \ \mathbf{u}_k)$ such that

$$\psi_{k+1} = \psi_k + T_s\Omega_k \quad (21)$$
$$\dot{z}_{k+1} = \dot{z}_k + T_s\,(g - F_k/m) \quad (22)$$
$$\omega_{k+1} = \omega_k + 5.89T_s(\Omega_k - \omega_k) \quad (23)$$
$$\sigma_{k+1} = \sigma_k + T_s\,(\dot{z}_k \sin\sigma_k/r^* - v_x\cos\sigma_k\cos\gamma_k/r^*) \quad (24)$$
$$\gamma_{k+1} = \gamma_k + T_s\,(v_x\sin\gamma_k/(r^*\sin\sigma_k) - \Omega_k) \quad (25)$$

where r^* denotes a fixed reference range value. Strictly speaking, (24) and (25) should include the induced image feature motion $\delta\sigma_k \propto 1/r$ and $\delta\gamma_k \propto 1/r$ due to the object movement. As the object motion is unknown this cannot be estimated. However, as the initial relative displacement is large, the induced motion will be small. At each instant, the visual predictive controller uses this model to find an optimal control action $\mathbf{u}_k^*$ corresponding to the minimum value of a quadratic cost function J_s^*, subject to a set of constraints. The resulting optimal control problem is solved over a prediction horizon N and can be defined as

$$J_s^*(\mathbf{s}_k, \bar{\mathbf{u}}_k) = \min_{\mathbb{U}} J_s(\bar{\mathbf{s}}_k, \bar{\mathbf{u}}_k) \quad (26)$$
$$\text{s.t.} \quad \bar{\mathbf{x}}_{k+1} = \mathbf{f}(\bar{\mathbf{x}}_k,\ \bar{\mathbf{u}}_k), \quad \forall k, \ldots, N_p - 1$$
$$\bar{\mathbf{x}}_k = \mathbf{x}_k$$

where $N_p = k + N$ and the objective function is given by

$$J_s(\bar{\mathbf{s}}_k, \bar{\mathbf{u}}_k) = (\bar{\mathbf{s}}_{N_p} \ominus \mathbf{s}^*)^T P(\bar{\mathbf{s}}_{N_p} \ominus \mathbf{x}^*) \quad (27)$$
$$+ \sum_{k}^{N_p-1} (\bar{\mathbf{s}}_k \ominus \mathbf{s}^*)^T Q(\bar{\mathbf{s}}_k \ominus \mathbf{s}^*) + \bar{\mathbf{u}}_k^T R\bar{\mathbf{u}}_k \quad (28)$$

The $\ominus$ denotes a modulo 2π subtraction required to bound the feature error and a bar denotes an internal controller variable. For example, $\bar{\mathbf{s}}$ denotes the image features calculated over the prediction horizon in order to calculate the optimal control action. In general, internal variables will not be the same as their true values due to model mismatch and added uncertainty. The diagonal weighting matrices are defined such that $Q \succ 0$, $R \succeq 0$ and $P \succeq 0$ where $\succ$ and $\succeq$ denote positive definiteness and semi-definiteness respectively. Notice that the objective function only considers the image features. This is equivalent to including the full state $\mathbf{x}_k$ in the objective function and setting the Q entries corresponding to the vehicle states to zero. The terminal penalty matrix P will penalize deviation from the reference image features at $k+N$. The set of constraints are given by

$$\mathbf{s}_k \in \mathbb{S} \subset \mathbb{R}^2, \quad \mathbb{S} \in [\mathbf{s}_{\min},\ \mathbf{s}_{\max}] \quad (29)$$
$$\mathbf{u}_k \in \mathbb{U} \subset \mathbb{R}^2, \quad \mathbb{U} \in [\mathbf{u}_{\min},\ \mathbf{u}_{\max}] \quad (30)$$
$$\mathbf{z}_k \in \mathbb{Z} \subset \mathbb{R}^3, \quad \mathbb{Z} \in [\mathbf{z}_{\min},\ \mathbf{z}_{\max}] \quad (31)$$

Visibility constraints (29) are handled with the application of a spherical camera, but are required to avoid the polar regions where (25) is undefined. The control (30) and state (31) constraints bound the controls and vehicle states respectively. They can be used to ensure the quadrotor motion remains inside a desirable region.

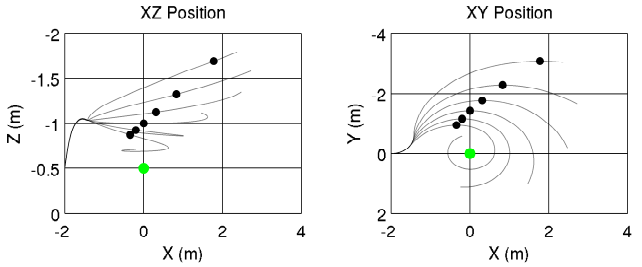

Fig. 8. Position in $\mathcal{F}_S$ for $\gamma^* \in [70\pi/180,\ 120\pi/180]$ at $10\pi/180$, $\sigma^* = 70\pi/180$ and $\psi^* = 0$. Black dots mark $\min J_s^*, \quad \forall\, k > 0$ and green dots denote the object position

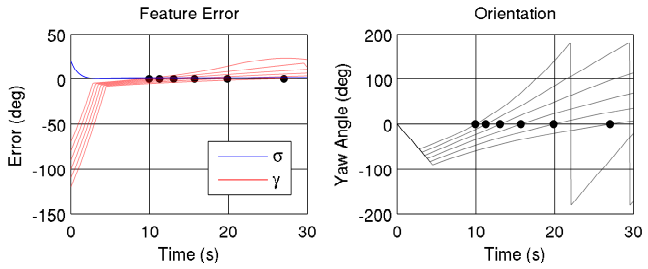

Fig. 9. Image feature error and yaw angle for $\gamma^* \in [70\pi/180,\ 120\pi/180]$ at $10\pi/180$, $\sigma^* = 70\pi/180$ and $\psi^* = 0$. Black dots mark $\min J_s^*, \quad \forall\, k > 0$

C. Resolution Decision - Stopping Spirals

A resolution decision or stopping criteria is required to cease the avoidance behaviour. If the spiral can be tracked, then the vehicle needs to be able to determine when to leave the spiral path and resume normal flight. If attempting to follow a reference spiral that cannot be obtained, the avoidance behaviour will also need to cease provided it is safe to do so. The decision should be coupled to the visual control to reduce the risk of premature stopping due to environmental disturbances such as turbulence [33]. If the decision is not coupled to the visual control, the avoidance behaviour may cease prior to establishing a safe spiral or at an inappropriate instant [26].

Consider the visual predictive controller using the objective function J_s for $\gamma^* \in [70\pi/180,\ 120\pi/180]$, $\sigma^* = 135\pi/180$ and $\mathbf{s}_0 = [\pi/2\ 0]$ as shown in Fig. 8. The spiral is tracked in all cases and the minimum of the objective function occurs when the vehicle returns to its initial heading as shown in Fig. 9. The value of the objective function can therefore be used to indicate an appropriate time to stop the avoidance behaviour, without relying on range. The approach is more robust than simply monitoring the heading angle [25], [26] due to the implicit coupling to the image feature values. To make the coupling explicit, now consider an augmented objective function J_ψ^* such that

$$J_\psi^* = J_s^* + \lambda \sum_{k}^{N_p} (\psi_k \ominus \psi_{k_d}) L(\psi_k \ominus \psi_{k_d}) \quad (32)$$
$$L = \max Q_{mn} \quad (33)$$

where λ is a positive scaling factor, ψ_{k_d} is the vehicle heading upon initial object detection and m and n represent row and column indexes respectively. The objective function is now directly dependant on the heading angle of the vehicle

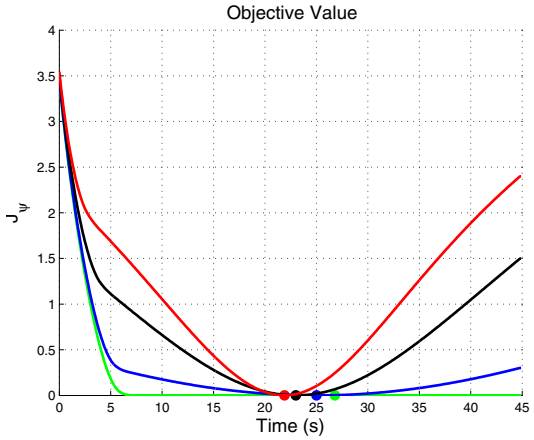

Fig. 10. Example objective function including minimums (*solid dots*) for simulations using J^*_ψ in the visual predictive controller and varying λ from 1 (*red*), 0.5 (*black*), 0.1 (*blue*) to 0.0 (*green*)

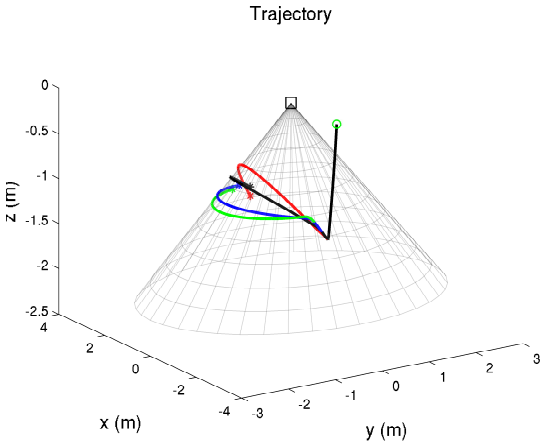

Fig. 11. Example trajectories for simulations using J^*_ψ in the visual predictive controller and varying λ from 1 (*red*), 0.5 (*black*), 0.1 (*blue*) to 0.0 (*green*)

which induces conflicting goals. Specifically, a tradeoff exists between establishing the reference spiral and maintaining heading, which can be managed using the scaling factor λ. For $\lambda = 0$, motion tends toward the reference spiral $\forall \mathbf{s}^*$. For $\lambda \neq 0$, motion is no longer on the true reference spiral as the trajectory becomes inclined. As λ increases, the resulting trajectories become more inclined, separation is reduced and the minimum objective function value occurs at an earlier instant. This is shown in Fig. 10-11.

To overcome this, J^*_s is used in the controller in order to derive the control commands that ensure a spiral trajectory, whilst J^*_ψ is calculated outside the controller and used to indicate when to stop the avoidance behaviour. This maintains the explicit coupling to the image features, without deviating from the reference spiral path. For the nominal case, the minimum objective function value $J^*_\psi = 0$ will occur when the spiral is established and the vehicle returns to its heading at first detection. This will not be possible in practise, due to added uncertainty and the possibility that the spiral may not be completely established for faster objects. A threshold ϵ needs to be applied to J^*_ψ to cease the avoidance behaviour. After such time, regular control can be resumed without requiring the visual predictive control input. If k_s

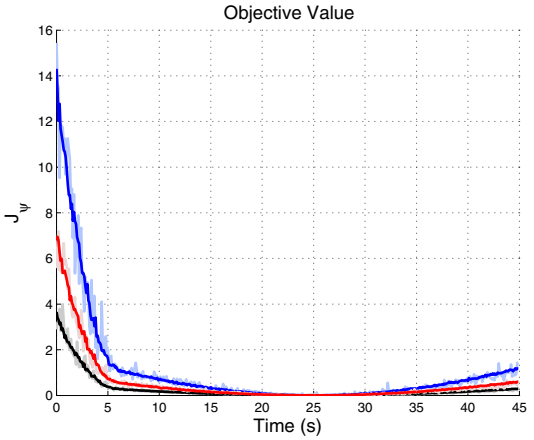

Fig. 12. Example objective function for simulations using varied weighting matrix magnitudes and feature noise characteristics. The magnitude is increased by a factor 1 (*black*), 2 (*red*) and then 4 (*blue*) for $\varsigma_s = 2\pi/180$ (*solid line*) and $\varsigma_s = 5\pi/180$ (*faded line*)

denotes the first time after k_d when $J^*_\psi \leq \epsilon$, the stopping criteria and associated control can then be defined such that

$$\text{Regular Control:} \quad \forall\, J^*_\psi, \quad 0 \leq k < k_d \quad (34)$$

$$\text{Avoidance Control:} \quad J^*_\psi > \epsilon, \quad k_d \leq k < k_s \quad (35)$$

$$\text{Regular Control:} \quad \forall\, J^*_\psi, \quad k_s \leq k < \infty \quad (36)$$

Another consideration is the magnitude of the weighting matrices P, Q and R. Provided the relative magnitude of the individual components remains the same, there is no effect on the time at which the objective function is a minimum, only the rate at which it converges to that point. Naturally, any noise is amplified in the objective function causing greater variations in the resulting value. The effect can be seen in Fig. 12, suggesting that the weighting matrix values should be kept small as the objective function will be thresholded.

V. Results

A. Simulation Framework

Simulations were conducted in MATLAB Simulink. A target trajectory generator was created to generate either a random encounter, a collision encounter or non-collision encounter. A set of KF were used to estimate vehicle states and a set of LQRI controllers were used to regulate forward and lateral velocity. A set of PID controllers were used to regulate the vertical rate and yaw rate to zero upon reaching the stopping threshold. The visual predictive controller used to guide spiral motion was implemented using the ACADO Toolkit [41]. A Sequential Quadratic Programming (SQP) approach employing an Active-Set strategy is used to solve the optimal control problem (26). ACADO also provides a MATLAB interface and optimized code for the visual predictive controller to be implemented on real platforms [33], [34]. An experimentally derived nonlinear point mass model was used to represent the vehicle dynamics. Importantly, the model used in the simulation environment includes experimentally derived delay terms [42], unlike the model used in the visual predictive controller. The sampling period for the image processing system T_i was assumed to be

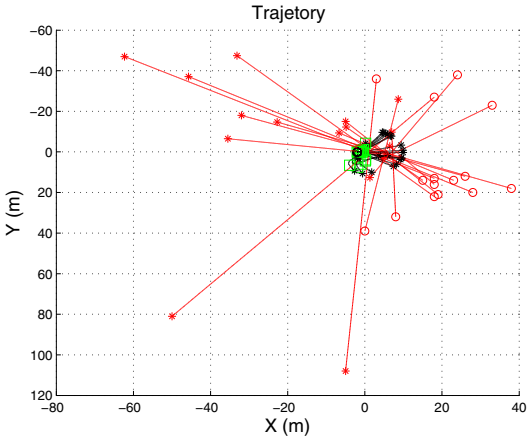

Fig. 13. Example simulations for 15 collision encounters. A planar representation is shown including the vehicle trajectories (*black*), target trajectories (*red*) and stopping instant k_s (*green squares*).

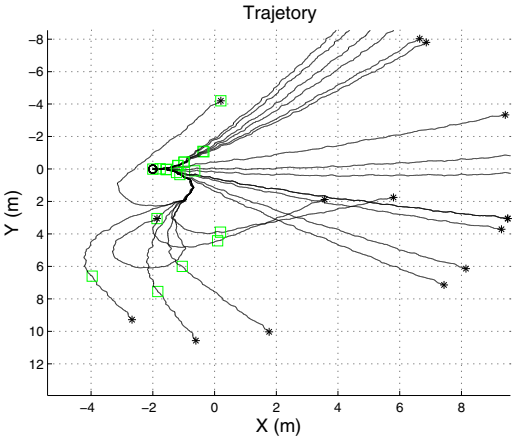

Fig. 15. Example simulations for 15 collision encounters focusing on vehicle trajectories (*black*) and stopping instant k_s (*green squares*). A planar representation is shown and the target trajectories have been removed.

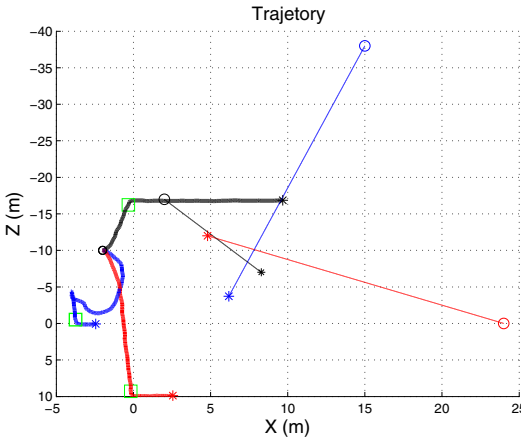

Fig. 14. Example simulations for 3 collision encounters in the xz-plane. Vehicle trajectories (*thick*), corresponding target trajectories (*thin*) and stopping instant k_s (*green squares*) are shown.

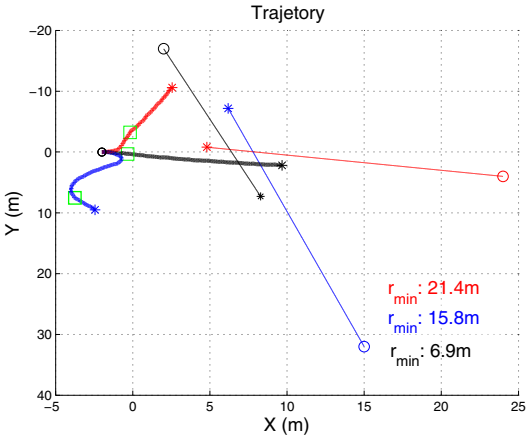

Fig. 16. Example simulations for 3 collision encounters in the xy-plane. Vehicle trajectories (*thick*), corresponding target trajectories (*thin*) and stopping instant k_s (*green squares*) are shown. Minimum range r_{min} is also included.

longer than that for the controller T_s. The prediction horizon $N = 10$ allows a solution to the minimization problem (26) to be found sufficiently fast, without compromising stability and control performance [43], [44]. Although the choice is arbitrary, a small prediction horizon can lead to stability issues resulting from aggressive control inputs whilst a large value increases the computational complexity.

The Simulink model includes environmental disturbances from turbulence $w_g(t)$ and ambient wind $w_a(t)$, added image feature noise $q_s(t)$ and imperfect actuation $q_c(t)$ as sources of uncertainty. All encounters were bounded by the time to closest approach t_{cpa}, initial range r_0 and object velocity. The simulation and control parameters are given in table II in the Appendix.

B. Simulation Trials

Multiple trials were performed to determine the effectiveness of the proposed avoidance strategy and stopping criteria, including over 500 collision and non-collision encounters. Example results for the collision encounters are illustrated in Fig. 13-16. Example results for the non-collision encounters are illustrated in Fig. 17-20.

For both collision and non-collision encounters only a few scenarios remain unresolved, as indicated by the green square and black star coinciding in Fig. 15 and 19. Although this behaviour is undesirable, the primary objective is to avoid collision, which is accomplished in these cases. In fact, the small number of collisions result from a fast moving target that is initially seen less than 3m from the vehicle. This type of situation presents a difficult encounter geometry for any control scheme given the vehicle performance limitations.

Consider a few examples for the collision encounters shown in Fig. 14 and 16. For the blue encounter, the object appears on the right and is allowed to cross, essentially giving way to the object. For the black encounter, the object has approached from the left and the vehicle has allowed the object to pass behind it. For the red encounter, an almost head-on scenario occurs and the vehicle avoids the object on the right. In all cases the appropriate avoidance decision was adopted, the stopping criteria was successful and the conflict is resolved. Now consider a few non-collision encounters shown in Fig. 18 and 20. The avoidance decision and stopping criteria has allowed increased separation without inducing a collision for each encounter. The vehicle then

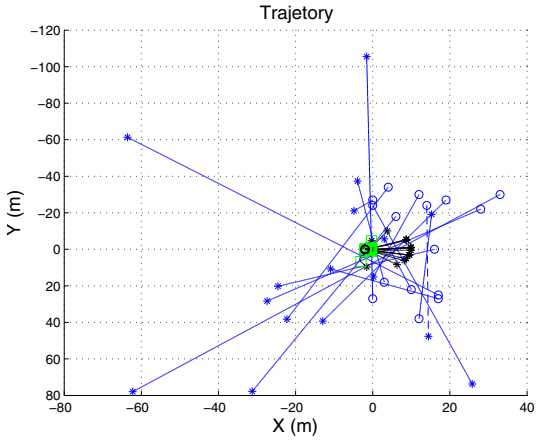

Fig. 17. Example simulations for 15 non-collision encounters. A planar representation is shown including the vehicle trajectories (*black*), target trajectories (*blue*) and stopping instant k_s (*green squares*).

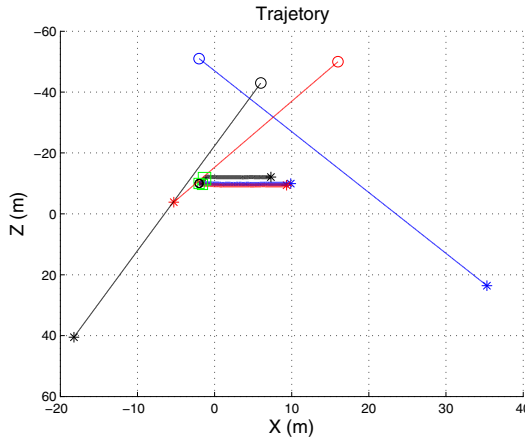

Fig. 18. Example simulations for 3 non-collision encounters in the xz-plane. Vehicle trajectories (*thick*), corresponding target trajectories (*thin*) and stopping instant k_s (*green squares*) are shown.

ceases precautionary avoidance behaviour relatively early, reducing the deviation from the reference flight path.

A summary of the outcomes for 1000 simulated encounters is provided in Table I, in which a collision is assumed if $\forall\ k > 0,\ r_{\text{min}} < 0.25$. A successful resolution indicates the collision was avoided and the stopping criteria was met such that for $k > k_d,\ \min J_\psi^* \leq \epsilon$, regardless of whether or not the reference spiral has been achieved. An unsuccessful resolution denotes an encounter in which the collision was avoided, but the stopping criteria was not met such that $\forall k > k_d,\ \min J_\psi^* > \epsilon$. In this case, the vision-based controller continually attempts to track a spiral about the object.

TABLE I
SIMULATION OUTCOMES

Encounter Type	**Collisions**	**Successful Resolution**	**Unsuccessful Resolution**	Total
Collision	14	442	44	500
Non-Collision	1	446	51	500

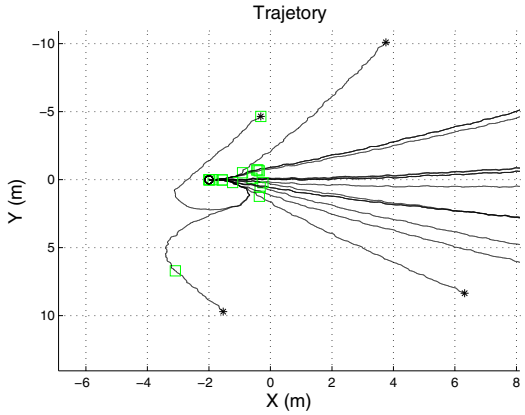

Fig. 19. Example simulations for 15 non-collision encounters focusing on vehicle trajectories (*black*) and stopping instant k_s (*green squares*). A planar representation is shown and the target trajectories have been removed.

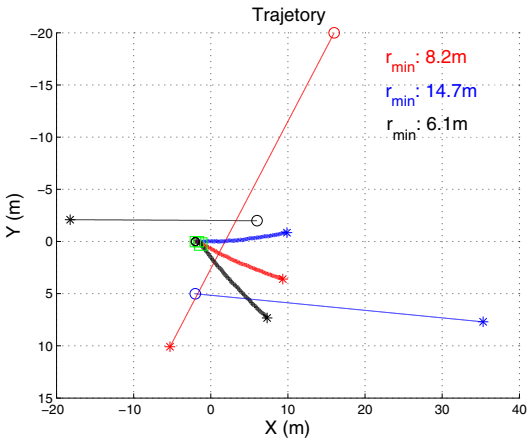

Fig. 20. Example simulations for 3 non-collision encounters in the xy-plane. Vehicle trajectories (*thick*), corresponding target trajectories (*thin*) and stopping instant k_s (*green squares*) are shown. Minimum range r_{min} is also included.

VI. CONCLUSIONS

This paper has presented a novel approach to uncooperative collision avoidance using vision-based control, intended for See and Avoid applications. An initial avoidance decision, based on regulatory guidelines and measurement uncertainty, provides the reference image features for a visual predictive control scheme. The controller is then able to provide collision avoidance and subsequent resolution using a range independent stopping criteria, overcoming typical state information limitations. Due to the adoption of regulatory guidelines, avoidance cannot be guaranteed for all encounters, but better predictability of the unmanned behaviour can be achieved. This is important considering the airspace must be shared with manned aircraft.

The approach considers all objects as potential threats, and relies on tuning two mutually exclusive thresholds to determine what action to take and when to cease the avoidance behaviour. This unique approach, although conservative, allows the consideration of additional outcomes from an automated collision avoidance system instead of assuming avoidance implies resolution. Additionally, the framework

resembles those of typical alerting systems using discrete decision thresholds, suggesting it is an ideal candidate for probabilistic performance assessments.

Further work includes extensions for other platform dynamics, including fixed wing, and subsequent performance analysis for larger scale problems.

VII. Appendix

A. Simulation Parameters

TABLE II
SIMULATION PARAMETERS

Parameter	Value	Units
T_c	$1/10$	s
T_c	$1/40$	s
N	10	-
Q	I_2	-
R	$10^{-8}I_2$	-
P	$2I_2$	-
λ	0.1	-
ϵ	0.15	-
ς_s	0.04	rad
$\varsigma_{\dot{s}}$	0.04	rad/s
t_{cpa}	$[5\ 55])$	s
r_0	$[0\ 40]$	m
v_t	$[-0.5\ 0.5]$	m/s
$w_g(t)$	$\mathcal{N}(\mathbf{0}_3, \mathbf{I}_3)$	rad/s
$w_a(t)$	$\mathcal{N}(\mathbf{0}_3, 0.25\mathbf{I}_3)$	m/s
$q_c(t)$	$\mathcal{N}(\mathbf{0}_2, 0.02\mathbf{I}_2)$	rad
$q_s(t)$	$\mathcal{N}(\mathbf{0}_2, \varsigma\mathbf{I}_2)$	N, rad/s
$\mathbf{u}_{max}$	$[7\ -10\pi/180]$	N, rad/s
$\mathbf{u}_{min}$	$[6\ 10\pi/180]$	N, rad/s
$\mathbf{s}_{max}$	$[20\pi/180\ -\pi]$	rad
$\mathbf{s}_{min}$	$[160\pi/180\ \pi]$	rad
$\mathbf{z}_{max}$	$[-1\ -2\pi\ -10\pi/180]$	m/s, rad, rad/s
$\mathbf{z}_{min}$	$[1\ 2\pi\ 10\pi/180]$	m/s, rad, rad/s
r^*	2	m
v	0.1	m/s

B. Regulations

Excerpt from Civil Aviation Safety Authority (CASA) Civil Aviation Regulations (CAR) 1998 [40]

161 Right of way

1) *CAR 161 (1) - An aircraft that is required by the rules in this Division to keep out of the way of another aircraft shall avoid passing over or under the other, or crossing ahead of it, unless passing well clear.*
2) *CAR 161 (2) - The pilot in command of an aircraft that has the right of way must maintain its heading and speed, but nothing in the rules in this Division shall relieve the pilot in command of an aircraft from the responsibility of taking such action as will best avert collision*

162 Rules for prevention of collision

1) *CAR 162 (1) - When 2 aircraft are on converging headings at approximately the same height, the aircraft that has the other on its right shall give way (with additional caveats for airships, gliders and balloons*
2) *CAR 162 (2) - When two aircraft are approaching head-on or approximately so and there is danger of collision, each shall alter its heading to the right*
3) *CAR 162 (3) - An aircraft that is being overtaken has the right-of-way and the overtaking aircraft, whether climbing, descending, or in horizontal flight, shall keep out of the way of the other aircraft by altering its heading to the right, and no subsequent change in the relative positions of the two aircraft shall absolve the overtaking aircraft from this obligation until it is entirely past and clear.*
4) *CAR 162 (4) - An overtaking aircraft shall not pass the aircraft that it is overtaking by diving or climbing*

163 Operating near other aircraft

1) *CAR 163 (1) - The pilot in command of an aircraft must not fly the aircraft so close to another aircraft as to create a collision hazard.*

References

[1] K. Dalamagkidis, K. Valavanis, and L. Piegl, "On unmanned aircraft systems issues, challenges and operational restrictions preventing integration into the national airspace system," *Progress in Aerospace Sciences*, vol. 44, no. 7-8, pp. 503-519, 2008

[2] F. Barfield, W. Res, D. Center, and A. Wright-Patterson, "Autonomous collision avoidance: the technical requirements," *IEEE National Aerospace and Electronics Conf. (NAECON'00)*, pp. 808-813, Oct. 2000

[3] C. Geyer, C. Singh, and S. Chamberlain, "Avoiding collisions between aircraft: state of the art and requirements for UAVs operating in civilian airspace," Technical Report: CMU-RI-TR-08-03, March 2008.

[4] Australian Transport Safety Bureau (ATSB), "Limitations of the see-and-avoid principle," Australian Government, Technical Report, November 2004.

[5] C. Morris "Midair collisions: limitations of the see-and-avoid concept in civil aviation," *Aviation, Space, and Environmental Medicine*, vol. 76, pp. 357-365, 2005.

[6] R. Kephart, "Comparison of see-and-avoid performance in manned and remotely piloted aircraft," Ph.D. dissertation, Ohio University, 2008.

[7] R. Carnie, R. Walker, P. Corke, "Image processing algorithms for UAV sense and avoid," *IEEE Int. Conf. Robotics and Automation (ICRA'06)*, pp. 2848-2853, May 2006

[8] J. Lai J. Ford L. Mejias and P. O'Shea, "Characterization of Sky-region Morphological-temporal Airborne Collision Detection," *Journal of Field Robotics*, pp. 171-193, vol. 30,No. 2, 2013

[9] J. Lai, L. Mejias, and J. Ford, "Airborne vision-based collision-detection system," *Journal of Field Robotics*, vol. 28, no. 2, pp. 137-157, March 2011.

[10] L. Mejias, S. McNamara, J. Lai, and J. Ford, "Vision-based detection and tracking of aerial targets for uav collision avoidance," *IEEE/RSJ Int. Conf. Intelligent Robots and Systems (IROS'10)*, pp. 87-92, Oct. 2010

[11] L. Mejias, J. Ford, and J. S. Lai, "Towards the implementation of vision-based uas sense-and-avoid," *Int. Congress of the Aeronautical Sciences (ICAS'10)*, Sep. 2010.

[12] O. Shakernia, M. Z. Chen, and V. M. Raska, "Passive ranging for uav sense and avoid applications,"*AIAA Infotech@Aerospace Conf. and Exhibit*, pp. 1-10, March 2005

[13] J. Zufferey, D. Floreano, "Toward 30-gram autonomous indoor aircraft: vision-based obstacle avoidance and altitude control," *IEEE Int. Conf. Robotics and Automation (ICRA'09)*, May 2009.

[14] O. Shakernia, J. Zvanya, A. White, N. Weingarten and V. Raska, "Sense and Avoid (SAA) flight test and lessons learned," *AIAA Infotech@Aerospace Conf. and Exhibit*, May 2007.

[15] W. Green, P. Oh, "Optic-flow-based collision avoidance," *IEEE Robotics & Automation Magazine*, vol. 15, no. 1, pp. 93-106, March 2008.

[16] A. Beyeler, J. Zufferey, and D. Floreano, "Vision-based control of near-obstacle flight," *Autonomous Robots*, vol. 27, pp. 201-219, July 2009.

[17] H. Choi, Y. Kim and I. Hwang, "Reactive collision avoidance of unmanned aerial vehicles using a single vision sensor," *Journal Guidance, Control and Dynamics*, vol. 36, no. 4, pp. 1234-1240, July-Aug. 2013

[18] S. Hutchinson, G. Hager, and P. Corke, "A tutorial on visual servo control," *IEEE Trans. Robotics and Automation*, vol. 12, no. 5, pp. 651-670, Oct. 1996.

[19] K. Boyadzhiev, "Spirals and conchospirals in flight of insects," *The College Mathematics Journal*, vol. 30, pp. 23-31, Jan. 1999.

[20] J. Lorimer, "Curved paths in raptorflight: deterministic models," *Journal of Theoretical Biology*, vol. 12, no. 4, pp. 880–889, Oct. 2006.

[21] J. Saunders and R. Beard, "Reactive vision based obstacle avoidance with camera field of view constraints," *AIAA Guidance, Navigation and Control Conf. and Exhibit*, 2008.

[22] J. Saunders and R. Beard, "Vision-based reactive multiple obstacle avoidance for micro air vehicles," *American Control Conf. (ACC'09)*, pp. 5253-5258, June. 2009.

[23] R. Sharma, J. Saunders, and R. Beard, "Reactive path planning for micro air vehicles using bearing only measurements," *Journal of Intelligent Robotic Systems*, vol. 65, pp. 409-416, Jan. 2012.

[24] L. Mejias, I. Mondragon, and P. Campoy, "Omnidirectional bearing-only see and avoid for small aerial robots," *IEEE Int. Conf. Automation, Robotics and Applications (ICARA'11)*, pp. 23-28, Dec. 2011

[25] A. Mcfadyen and L. Mejias, "Visual servoing approach to collision avoidance for aircraft," *Int. Congress of the Aeronautical Sciences (ICAS'12)*, Sep. 2012.

[26] A. Mcfadyen, P. Corke and L. Mejias, "Rotorcraft collision avoidance using spherical image-based visual servoing and single point features," *IEEE/RSJ. Int. Conf. Intelligent Robots and Systems (IROS'12)*, pp. 1199-1205, Oct. 2012.

[27] H. Yu, R. Sharma, R. Beard and C. Taylor, "Observability-based local path planning and collision avoidance for micro air vehicles using bearing-only measurements," *American Control Conf. (ACC'11)*, pp. 4649-4654, July 2011

[28] H. Yu, R. Sharma, R. Beard and C. Taylor, "Observability-based local path planning and obstacle avoidance using bearing-only measurements," *Journal Robotics and Autonomous Systems*, vol. 61, no. 12, pp. 1392-1405, Dec. 2013

[29] X. Yang, L. Mejias, and T. Bruggemann, "A 3D collision avoidance strategy for uavs in an non-cooperative environment," *Journal of Intelligent Robotic Systems*, vol. 70, No. 1-4, pp. 315-327, April 2013.

[30] R. Findeisen and F. Allgower, "An introduction to nonlinear model predictive control," *21st Benelux Meeting on Systems and Control*, pp. 119-218, 2002.

[31] A. Allibert, E. Courtial, and F. Chaumette, "Predictive control for constrained image-based visual servoing," *IEEE Trans. Robotics*, vol. 26, no. 5, pp. 933-939, Oct. 2010

[32] D. Lee, H. Lim, and H. Kim "Obstacle avoidance using image-based visual servoing integrated with nonlinear model predictive control," *IEEE Int. Conf. Decision and Control (CDC'11)*, pp. 5689-5694, Dec. 2011.

[33] A. Mcfadyen, L. Mejias, P. Corke and C. Predalier, " Aircraft collision avoidance using visual predictive control and single point features," *IEEE Int. Conf. Intelligent Robotics and Systems (IROS'13)*, pp. 50-56. Nov. 2013

[34] A. Mcfadyen, P. Corke and L. Mejias, "Visual predictive control of spiral motion," *IEEE Trans. Robotics* (*Cond. Accepted*).

[35] C. Geyer and K. Daniilidis, "A unifying theory for central panoramic systems and practical implications," *European Conf. Computer Vision (ECCV'08)*, pp. 445-461, June 2000

[36] P. Corke, "Spherical image-based visual servo and structure estimation," *IEEE Int. Conf. Robotics and Automation (ICRA'10)*, pp. 5550-5555, Sep. 2010

[37] B. Fajen and W. Warren, "Behavioural dynamics of steering, obstacle avoidance, and route selection," *Journal of Experimental Psychology-Human Perception and Performance*, vol. 29, no. 2, pp. 343-361, 2003.

[38] M. Kochenderfer, J. Griffith, and J. Kuchar, "Hazard alerting using line-of-sight rate," *AIAA Guidance, Navigation and Control Conf. and Exhibit*, Aug. 2008.

[39] T. Bruggemann and L. Mejias, "Airborne collision scenario flight tests: impact of angle measurement errors on reactive vision-based avoidance control," *Australian Int. Aerospace Conf. (AIAC'13)*, Feb. 2013.

[40] Civil Aviation Safety Authority (CASA), Civil Aviation Regulations (CAR) 1988, Part 12, Section 162-163, 1988

[41] B. Huska and H. Ferreau and M. Diehl, "ACADO Toolkit - an open source framework for automatic control and dynamic optimization," *Optimal Control Theory and Methods*, vol. 32, No. 3, pp. 298-312, 2011.

[42] M. Burri, Y. Nikolic, C. Hurzeler, G. Caprari and R. Siegwart "Aerial service robots for visual inspection of thermal power plant boiler systems," *Int. Conf. Applied Robotics for the Power Industry*, 2012

[43] D. Mayne, J. Rawlings, C. Rao and M. Scokaert, "Constrained model predictive control: stability and optimality," *Automatica*, vol. 36, No. 6, pp. 789-814, June 2000.

[44] J. Garriga, M. Soroush, "Model predictive control tuning methods:a review," *Ind. Eng. Chem. Res.*, vol. 49, no. 8, pp. 3505-3515, 2010